Optimalization of T_c in NbN-films

J.M. van der Knaap

Leiden, November 2006

Contents

Chapter 1

Introduction

Superconductivity was discovered in 1911. It was found that below a certain temperature the current is able to flow without dissipation through the material. This temperature depends on the material which is used and is called critical temperature (T_c). It can be far below 1 K as well as higher than 100 K for a high T_c superconductor.
In this project 2 materials were used. The first one is NbN. NbN is a material with a relatively high T_c (17 K maximum). It consists of niobium (Nb) and nitrogen (N), in equal amounts in the ideal case. It can be made by reactive sputtering, by adding N_2 to the Ar sputter gas. The amount of N in the resulting NbN sample and therefore T_c of the resulting sample depends on the N_2 pressure used during sputtering. The second material is MgB_2. This is a layered anisotropic material with a high T_c (39 K).
The first purpose of this project is to enhance the T_c of NbN. It was already possible to make NbN in the Z400, a standard sputter machine with a base pressure of about 10^{-6} mbar. The T_c of this material was 10.5 K. It was thought that the T_c would become higher if a UHV system was used (UHV means ultra high vacuum, base pressure was about 10^{-9} mbar.), because there will be less contamination. Contamination, especially with O_2, would lower the T_c. In the UHV system samples are made under various conditions, by varying the Ar and N_2 pressure and using DC and RF power supplies. T_c was checked by measuring R-T curves. Also some first results could be obtained by film deposition in the ATC, a new sputter machine where the substrates can be heated (base pressure of the ATC: about 10^{-8} mbar).
The second purpose was to check the T_c of a MgB_2 sample. Both types of samples were investigated by measuring the resistance (R) as function of temperature (T). This also yielded ρ_0, the resistivity just above T_c, as a parameter to characterize samples.

Structure of the report The theory necessary for the report will be presented in chapter 2. A description of the used materials together with the methods of sample preparation and characterization will be described in chapter 3. The NbN results will be shown in chapter 4. The conclusion is written in chapter 5. The results for the MgB_2 sample are given in the appendix .

Chapter 2

Theory

2.1 Introduction to superconductivity

Superconductivity was discovered in 1911[1] [1]. It was found that the resistance of a Hg sample drops to 0 in the vicinity of 4.2 K (see fig. 2.1). So superconductivity can be characterized by infinite conductivity. This is the first characteristic. The second one is perfect diamagnetism. A magnetic field is totally excluded from the sample if the sample is cooled through T_c. This is called the Meissner effect [3]. It is not explained by infinite conductivity nor does perfect diamagnetism imply infinite conductivity. The expulsion of the magnetic field does not occur for arbitrarily large fields. Superconductivity is destroyed above a critical field H_c. If a field higher than H_c is applied, the sample is not superconducting anymore. H_c is also dependent on temperature. Exactly at T_c H_c is in fact 0 and it reaches a finite field at 0 K.
These properties of a superconductor can be described using the London equations [4]. They are purely phenomenological. It is not explained why they should be true but they correctly describe the response of a superconductor to a magnetic field. The equations are

$$E = \frac{\partial}{\partial t}(\Lambda J_s) \tag{2.1}$$

$$h = -c\nabla \times (\Lambda J_s) \tag{2.2}$$

where

$$\Lambda = \frac{4\pi\lambda^2}{c^2} = \frac{m}{n_s e^2} \tag{2.3}$$

[1]The material in the following 3 sections was taken from reference [2]

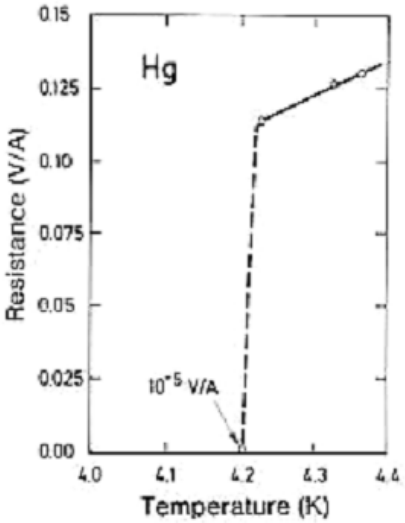

Figure 2.1: R vs. T for Hg as measured in 1911

n_s is the density of superconducting electrons. It was assumed that not all electrons in a material would become superconducting electrons but only a certain amount. These equations lead to the idea of a penetration depth λ. This is the depth to which the field can penetrate the superconductor. Another useful parameter is ξ, the coherence length. The coherence length is roughly speaking the distance in which variations in the density of superconducting electrons can occur. It is not found in the London theory, since this early theory does not take the quantum nature of superconductivity into account. Two other theories which do this are the BCS-theory developed by J. Bardeen, L. N. Cooper and J. R. Schrieffer [6][7] and the Ginzburg-Landau theory [8] and in both theories ξ naturally occurs as a characteristic length scale. The two next sections are devoted to these.

2.2 BCS-theory

In a metal the electrons can be depicted as decoupled from the lattice. The lattice can move much slower than the electrons. For many applications the ions can be depicted as not moving at all. The electrons then move through a periodic static lattice. In a perfect periodic lattice they cannot be scattered and therefore has a perfect lattice no resistance. But perfect lattices do not exist in practice. A real lattice is distorted by thermal vibrations and lattice

defects and this causes resistance. But for simplicity a metal is described as a perfect lattice with electrons moving freely through it. Each electron has a certain momentum **p**. It is not possible for 2 electrons with the same spin to have the same **p** because the Pauli exclusion principle forbids that. So for the state with the lowest energy the states with the lowest p values have to be filled up to a certain level. All occupied states are inside the Fermi sphere. All states outside the Fermi sphere are unoccupied (at 0 K). This is the ground state. At lower temperatures the metal can go into a new state. It then becomes a superconductor. A superconductor has a different ground state. It achieves this by pairing electrons into Cooper pairs.

2.2.1 Cooper-pairs

In a normal metal the resistance is caused by phonons (quantized lattice vibrations) and lattice defects. In a superconductor it are phonons that cause the electrons to have zero resistance. In the description of a metal it was assumed that the electrons do not interact with the lattice. But that is an approximation. When an electron moves through the lattice the ions are a bit attracted by the electron (see fig. 2.2). This causes a positive charge on that site. It is imaginable that other electrons are attracted by this positive charge. In this way 2 electrons can couple and form a pair. This is called a Cooper pair. The electrons in a Cooper pair are in general quite far apart, a few nm or μm depending on the material where they live in. To have the lowest energy possible the electrons in a Cooper pair have equal and opposite momenta and opposite spin.
That the lattice is involved in the formation of a Cooper pair can be concluded from the isotope effect. It says that different isotopes of the same material have a different T_c. The dependence goes as

$$T_c \sim \frac{1}{\sqrt{M}} \tag{2.4}$$

where M is the isotopic mass.

2.2.2 BCS-theory

The BCS theory is most easily described in language of the theory of second quantization. In this theory particles are described in terms of raising operators ($c_k^\dagger$) and lowering operators (c_k).

$$H = \sum_{k\sigma} \varepsilon_k n_{k\sigma} + \sum_{kl} V_{kl} c_{k\uparrow}^\dagger c_{-k\downarrow}^\dagger c_{-l\downarrow} c_{l\uparrow} \tag{2.5}$$

Figure 2.2: electron interacting with lattice

ε_k is the unperturbed plane wave energy, n is the number of particles and V is the interaction potential. If we write $c_{-k\downarrow}c_{k\uparrow} = b_k + (c_{-k\downarrow}c_{k\uparrow} - b_k)$ this becomes

$$H_M = \sum_{k\sigma} \xi_k c^\dagger_{k\sigma} c_{k\sigma} + \sum_{kl} V_{kl}(c^\dagger_{k\uparrow} c^\dagger_{-k\downarrow} b_l + b^\dagger c_{-l\downarrow} c_{l\uparrow} - b^\dagger_k b_l) \tag{2.6}$$

with b_k to be determined. ξ_k is now the energy with respect to the Fermi energy: $\xi_k = \varepsilon_k - E_F$. Define:

$$\Delta_k = -\sum_l V_{kl} b_l = -\sum_l V_{kl} < c_{-k\downarrow} c_{k\uparrow} > \tag{2.7}$$

Δ is the energy gap of the electrons. This can be inserted in equation 2.6 and results in

$$H_M = \sum_{k\sigma} \xi_k c^\dagger_{k\sigma} c_{k\sigma} - \sum_k (\Delta_k c^\dagger_{k\uparrow} c^\dagger_{-k\downarrow} + \Delta_k c_{-k\downarrow} c_{k\uparrow} - \Delta_k b^\dagger_k) \tag{2.8}$$

Now a Bogoliubov transformation is performed:

$$c_{k\uparrow} = u^\dagger_k \gamma_{k0} + v_k \gamma^\dagger_{k1} \tag{2.9}$$

$$c^\dagger_{-k\downarrow} = -v^\dagger_k \gamma_{k0} + u_k \gamma^\dagger_{k1} \tag{2.10}$$

Insert this and choose u_k and v_k so as to diagonalize H_M. The remaining terms are:

$$H_M = \sum_k (\xi_k - E_k + \Delta_k b^\dagger_k) + \sum_k E_k(\gamma^\dagger_{k0}\gamma_{k0} + \gamma^\dagger_{k1}\gamma_{k1}) \tag{2.11}$$

This leads to

$$\Delta_k = -\sum_l V_{kl} < c_{-l\downarrow} c_{l\uparrow} >= -\sum_l V_{kl} u_l^\dagger v_l < 1 - \gamma_{l0}^\dagger \gamma_{l0} - \gamma_{l1}^\dagger \gamma_{l1} > \quad (2.12)$$

The term between <> represents excitations which is in case of thermal excitation just $1 - f(E_k)$ where $f(E_k)$ is the Fermi function.So equation 2.12 becomes

$$\Delta_k = -\sum_l V_{kl} u_l^\dagger v_l (1 - 2f(E_k)) = -\sum_l V_{kl} \frac{\Delta_l}{2E_l} \tanh \frac{\beta E_l}{2} \quad (2.13)$$

where β is $\frac{1}{k_B T}$, the inverse temperature. To proceed it is necessary to specify V_{kl}. BCS used the approximation that V_{kl} is a constant if $|\xi_k|$ and $|\xi_l| < \hbar\omega_D$ and 0 otherwise (ω_D is the Debye frequency). Note that is not necessary to specify where this potential comes from, but in conventional superconductors it is the electron phonon coupling. Using $V_{kl} = -V$ equation 2.13 becomes

$$\frac{1}{V} = \frac{1}{2} \sum_k \frac{\tanh(\beta E_k/2)}{E_k} \quad (2.14)$$

This equation can be solved for β if the sum is converted into an integral, the variable is changed and the symmetry is taken into account.

$$\frac{1}{N(0)V} = \int_0^{\beta_c \hbar\omega_D/2} \frac{\tanh x}{x} dx = \ln(\frac{2\gamma}{\pi} \beta_c \hbar\omega_D) \quad (2.15)$$

where γ is Euler's constant and $N(0)$ is the density of states at the Fermi surface. This equation can be solved and results in the following equation for T_c:

$$k_B T_c = \beta_c^{-1} = 1.13 \hbar\omega_D e^{\frac{-1}{N(0)V}} \quad (2.16)$$

This is an equation for T_c. Since actually T_c is the parameter which is easiest to measure and V is difficult to calculate, it is not possible to calculate T_c with this equation. Instead, from T_c measurements conclusions can be drawn about N(0), V and ω_D. It is easy to see how T_c depends on N(0), V and ω_D. T_c increases as N(0) increases, V increases or ω_D increases.

2.3 Type I and Type II superconductors

The complete Meissner effect is only displayed by a type I superconductor. In this type superconductors the applied magnetic field is completely expelled from the superconductor if the temperature is lower than T_c. If the magnetic field is higher than H_c the field can penetrate and the superconductivity is destroyed. In a type II superconductor the field is also expelled from the material but only below a certain critical field H_{c1}. If the field is higher than H_{c1} but below a second critical field H_{c2} the field is allowed to enter the superconductor but only in flux tubes. Each tube can carry a flux quantum

$$\Phi_0 = \frac{h}{2e} \tag{2.17}$$

The flux tubes are not superconducting. If the field is higher than H_{c2} the superconductor becomes normal and the superconductivity is destroyed. H_{c2} for a type II superconductor is in general higher than H_c for a type I superconductor. In general superconducting elements exhibit type I behavior and alloys type II behavior.

2.4 Ginzburg-Landau-theory

Ginzburg-Landau theory is used to deal with situations where Δ is not constant in space but varies. These problems could be solved using BCS theory as well, but this becomes mathematically very difficult. So it is more helpful to use the more macroscopic Ginzburg-Landau theory. It is in fact only applicable near T_c and based on the theory Landau developed for second order phase transitions. This theory expands the free energy, which should be always in a minimum, in powers of an order parameter. Ginzburg-Landau uses also a order parameter which is in general complex. Near T_c the free energy density can be expanded as

$$f = f_{n0} + \alpha|\Psi|^2 + \frac{\beta}{2}|\Psi|^4 + \frac{1}{4m}\left|\left(\frac{\hbar}{i}\nabla - \frac{2e}{c}\overrightarrow{A}\right)\Psi\right|^2 + \frac{h^2}{8\pi} \tag{2.18}$$

f_{n0} is the free energy density in the normal state and in zero field, α and β are parameters and Ψ is the order parameter. $\overrightarrow{A}$ is the vector potential and h is the magnetic field. Because the order parameter is in general complex the expansion uses powers of $|\Psi|^2$ instead of powers of Ψ as the free energy should stay real. The order parameter is defined as

$$n_s = |\Psi|^2 \tag{2.19}$$

where n_s is the density of superconducting electrons. It is 0 in the normal state. For the theory to make sense, the parameter α has to be 0 at T_c and negative as $T<T_c$. So we can write

$$\alpha(t) \propto \alpha'(t-1) \tag{2.20}$$

where t=T/T_c. The parameter β can be taken positive and independent of temperature. Equation 2.18 can be solved by setting $df/d\Psi = 0$. This leads to the Ginzburg-Landau differential equations (to be used with suitable boundary conditions):

$$\alpha\Psi + \beta|\Psi|^2\Psi + \frac{1}{4m}\Big(\frac{\hbar}{i}\nabla - \frac{2e}{c}A\Big)^2\Psi = 0 \tag{2.21}$$

$$J = \frac{e\hbar}{2mi}\Big(\Psi^\dagger\nabla\Psi - \Psi\nabla\Psi^\dagger\Big) - \frac{2e^2}{mc}|\Psi|^2 A \tag{2.22}$$

It is now useful to define two other parameters:

$$\xi^2 = \frac{\hbar^2}{4m|\alpha(t)|} \propto \frac{1}{1-t} \tag{2.23}$$

$$\lambda^2 = \frac{mc^2\beta}{8\pi e^2|\alpha(t)|} \tag{2.24}$$

ξ represents the characteristic length for variations of Ψ and is called the coherence length. λ is the field penetration depth.

$$\kappa = \lambda/\xi \tag{2.25}$$

As ξ and λ have approximately the same temperature dependence κ is independent of temperature. κ can be used to distinguish type I and type II superconductors. For type I superconductors $\kappa < 1/\sqrt{2}$ and for type 2 superconductors $\kappa > 1/\sqrt{2}$. If the value for κ is large, the (type II-) superconductor can gain energy in a not too large magnetic field by letting the field penetrate in small flux tubes. A type I superconductor does not gain energy in this way.

2.4.1 Coherence length

To obtain a equation for the coherence length in terms of measurable quantities, we can use the linearized GL equations. They are obtained by dropping the term $\beta|\Psi|^2\Psi$. This is allowed if $|\Psi|^2$ is not too large. This results in:

$$\alpha\Psi + \frac{1}{4m}\Big(\frac{\hbar}{i}\nabla - \frac{2e}{c}A\Big)^2 = 0 \tag{2.26}$$

Using this equation the following equation for H_{c2} can be derived:

$$H_{c2} = \frac{\Phi_0}{2\pi\xi^2(T)} \tag{2.27}$$

The temperature dependence of the coherence length is given by (see equation 2.23)

$$\xi(T) = \frac{\xi(0)}{\sqrt{1 - T/T_c}} \tag{2.28}$$

This equation can be substituted in equation 2.27. Differentiating with respect to T gives as equation for $\xi(0)$

$$dH_{c2}/dT = \frac{-\Phi_0}{2\pi T_c \xi^2(0)} \Rightarrow \xi^2(0) = \frac{-\Phi_0}{2\pi T_c dH_{c2}/dT} \tag{2.29}$$

Equation 2.29 is used to calculate $\xi(0)$ for all the samples that have been measured.

Chapter 3

Materials, sample preparation and characterization

In this chapter I discuss some basic properties of the materials which are to be investigated, NbN and MgB_2, as well as the sample preparation and characterization methods.

3.1 NbN-lattices

There are 12 phases of NbN [9][10] (see fig.3.1 for an idea of the phase diagram.). They have all a different concentration of N and a different T_c. They are listed in order of increasing nitrogen-concentration.

α-NbN The α-phase of NbN consists of interstitial N-atoms in the Nb(=bcc)-lattice. The lattice parameter is a=0.3294 nm.

β-NbN (Nb_2N) β-NbN has a hexagonal (ϵ-Fe_2N-type) lattice. The lattice parameters are a=0.305 nm and c=0.496 nm. T_c is lower than 1.2 K.

γ-NbN (Nb_4N_3) Nb_4N_3 has a face centered tetragonal lattice (distorted NaCl-type). The lattice parameters are a=0.438 nm and c=0.868 nm. T_c is 8.9 K [9] or 11.5 K [13].

δ-NbN δ-NbN has an fcc-lattice (NaCl-structure). In fact, it is NbN_x with x=0.88-0.98 or 1.015-1.062. The exact stoichiometric composition is not stable. The lattice parameter is 0.438 nm. T_c is 17.3 K. This is the highest T_c in the Nb-N system and therefore this is the desired phase.

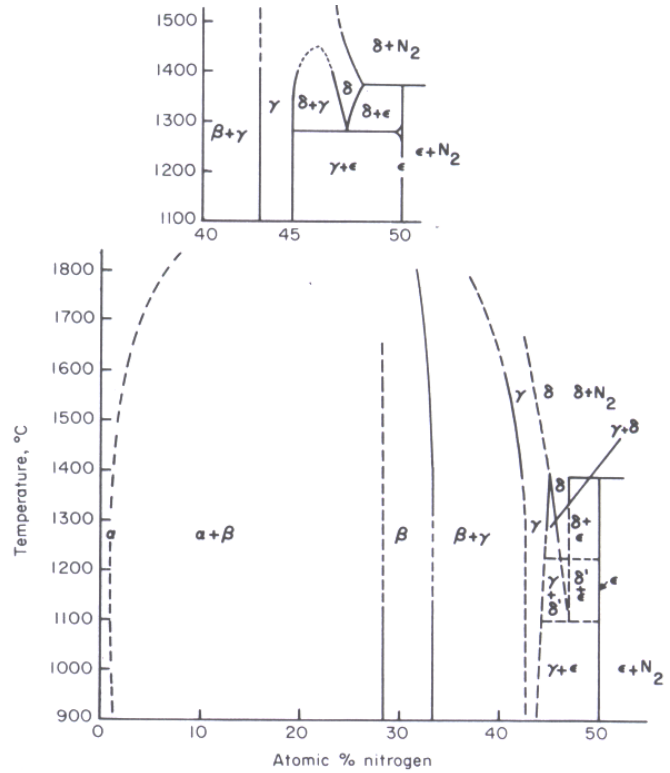

Figure 3.1: phase diagrams for NbN. The lower diagram is Brauer's proposal given originally by Brauer and Esselborn [11] and then modified by him [12]. The subsequent modification by Guard et al. [12] of the nitrogen-rich side is shown in the upper diagram. Not all unstable phases are indicated. The figure was taken from [9].

ϵ-NbN ϵ-NbN has a hexagonal (TiP-type) lattice. The lattice parameters are a=0.2958 nm and c=1.127 nm. T_c is lower than 1.77 K.

Nb_3N_3 This phase has a fcc-lattice with 25% of the atoms removed (NbO-structure). T_c is 16.4 K. [13]

Nb_5N_6 This phase has a hexagonal lattice. The lattice parameters are a=0.5193 nm and c=1.038 nm. T_c is very low (as ϵ-NbN).

Nb_4N_5 This phase has a tetragonal lattice. The lattice parameters are a=0.6853 nm and c=0.427 nm. T_c is 8.0-8.5 K. [14]

δ-NbN is not stable below 1370 °C. The transition $\delta \rightarrow \epsilon$ is possible. In this transition, the following (metastable) phases are possible (in this order)[15]:

(N-vacancy)ordered δ-NbN This phase has a tetragonal lattice.

ordered ζ-NbN This phase has a hexagonal lattice.

ordered γ'-NbN This phase has a monoclinic lattice

δ'-NbN δ'-NbN has a hexagonal (anti-NiAs-type) lattice with lattice parameters a=0.2968 nm and c= 0.535 nm.

In practice these phases are not very important as they are not stable. In summary, the more cubic the phase is, the higher the T_c. Hexagonal NbN phases have no or a very low T_c. The desired phase is the cubic δ-NbN phase, because it has the highest T_c. The difficulty in sputtering NbN is that this phase is metastable at room temperature. So sputtering without precautions can cause the wrong phases to occur and results in low T_c. This can be avoided by sputtering at higher temperatures or addition of carbon, usually by adding methane to the sputter gas. NbC itself has not a very high T_c (11 K), but it stabilizes the NbN lattice and causes therefore a high T_c. The composition $NbC_{0.3}N_{0.7}$ gives the highest T_c (17.8 K) [16]. In fig. 3.2 - fig. 3.6 simulations of 5 X-ray-diffraction spectra for various NbN compounds are given. As can be seen the spectra are very similar to each other. This causes difficulties when trying to determine the crystal structure by X-ray-diffraction, especially if the layers are thin, as in that case only the highest peaks are visible.

3.2 T_c-dependence on lattice constants of NbN

T_c was given by equation 2.16:

$$kT_c = 1.13\hbar\omega_D e^{\frac{-1}{N(0)V}}$$

It says that T_c depends on the density of states at the Fermi surface $N(0)$, the attractive potential V and the Debye frequency ω_D. V is the average of $V_{k,k'}$ at the Fermi surface. $N(0)$ and V are the most important ones as they occur in a power of e. So ω_D can be ignored.
The question arises why NbN has such relatively high T_c (17 K compared

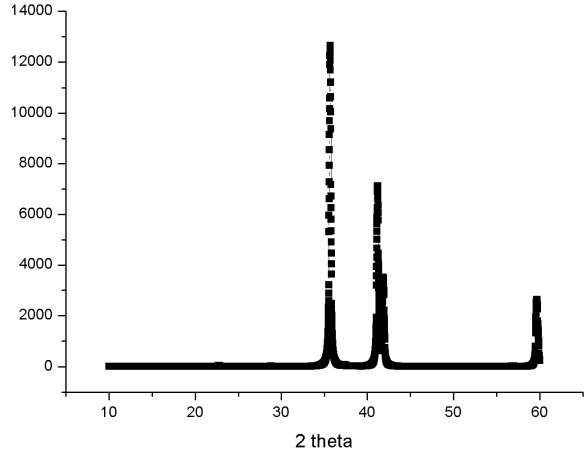

Figure 3.2: simulation of X-ray-diffraction for Nb_4N_3.

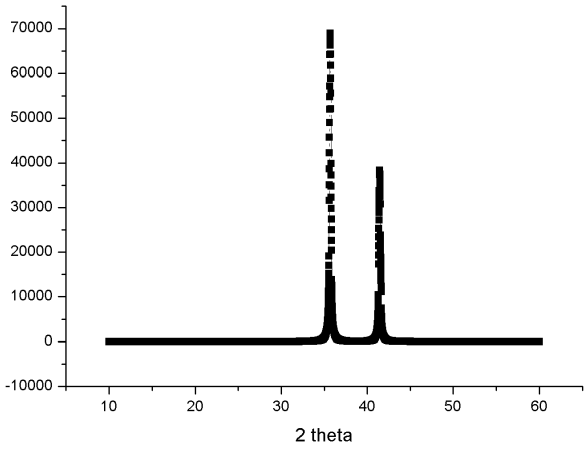

Figure 3.3: simulation of X-ray-diffraction for δ-NbN.

to 9 K for pure Nb). It can be shown that the density of states in NbN is actually low compared to that of pure Nb. So we have to look at V, that is in this case the electron-phonon-coupling. The strong electron-phonon coupling is due to the small mass of the light nitrogen atom [17]. The mass of N is so much smaller than that of Nb that it can counteract a reduction in

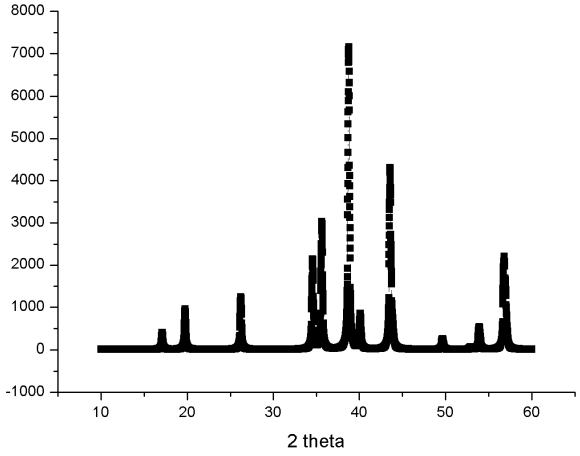

Figure 3.4: simulation of X-ray-diffraction for Nb_5N_6.

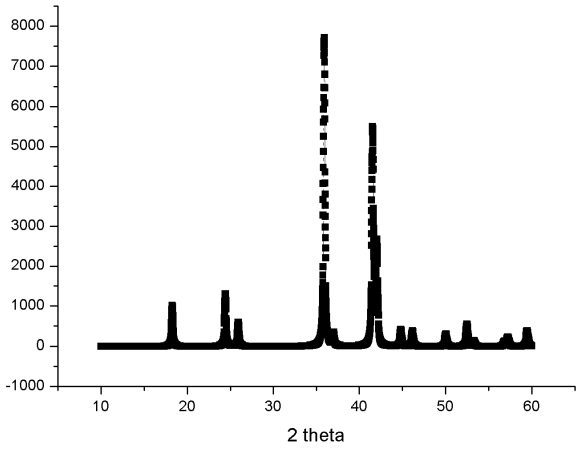

Figure 3.5: simulation of X-ray-diffraction for Nb_4N_5.

the density of states and scattering power with respect to Nb. The N atoms scatter electrons at the Fermi energy very strongly, so this can give rise to strong electron-phonon interactions. Under certain circumstances the consequence of small mass of N is that the light element oscillates with a large amplitude about its equilibrium position. Provided that it scatters electrons

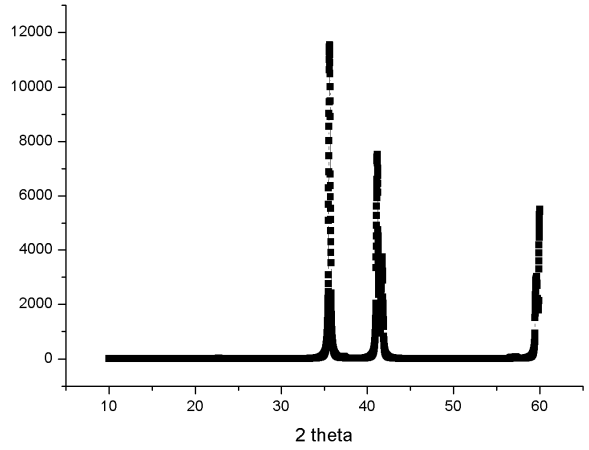

Figure 3.6: simulation of X-ray-diffraction for tetragonal δ-NbN.

at the Fermi energy sufficiently strongly the light element will give a large contribution to the electron phonon coupling.
Since the largest amplitude oscillations are likely to occur near lattice instabilities, it seems natural to find the highest T_c's in those compounds whose structure is near such instability. It is suggested that the high T_c comes from lattice instabilities. These instabilities are signalled by abnormalities in bond lengths. It works like this: if we look at materials with high T_c's, our attention is limited to materials with large values for the electron phonon coupling. Because of these large values the ion-ion interactions are screened by the electron-ion interactions. This gives rise to lattice instabilities, which can be removed by altering the bond lengths to abnormal values. In many cases, this alteration causes a lowering of the symmetry of the crystal and a reduction of the electronic density of states. This lowers the T_c. In other cases the instable lattice is stabilized and in this case the T_c can be anomalously high.

This is probably the case in NbN as can be seen from examining the system NbX with X=C,N or O. If one plots the lattice constant for NbX with X=C,N,O the line through the points should be linear (Vegard's law). In the NbX system this is not the case. NbN has the highest T_c in this system as can be seen in fig. 3.7 and NbN is at the point where the relationship between lattice constant and X is not linear. Apparently NbN is close to a phase-transition and is not very stable. The high T_c is caused by the large oscillations of the N atoms. But the oscillations cannot be arbitrarily large.

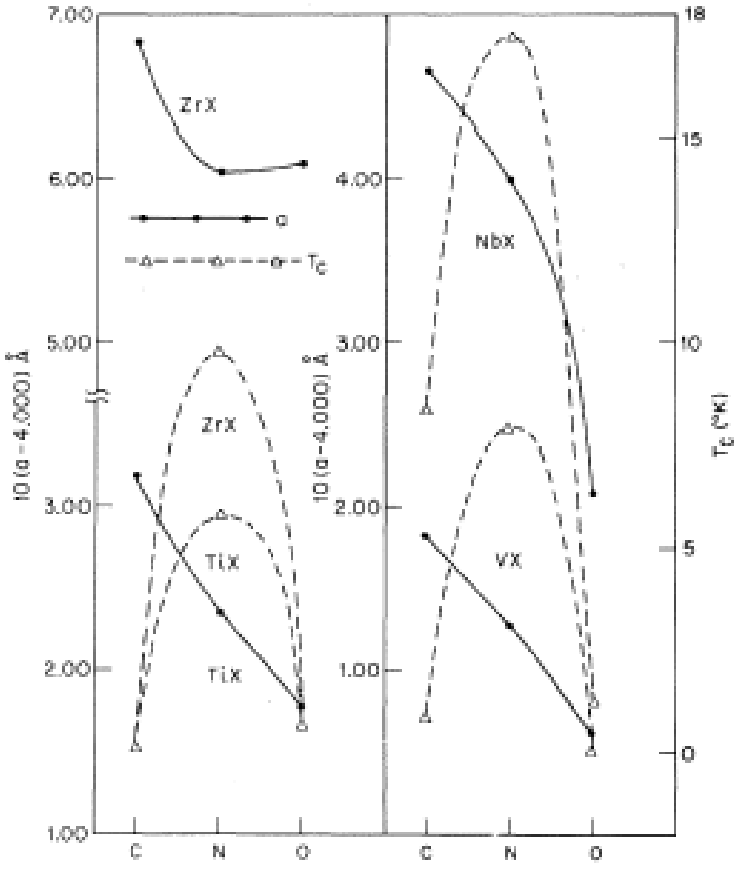

Figure 3.7: Lattice constants (solid lines) and T_c (dashed lines) for RX compounds in NaCl structure (R=Zr, Ti, Nb, V and X=C, N, O). The highest values for T_c occur for X=N. There is no linear relationship between the lattice constants of RX. (Figure taken from ref. [17])

They will be stabilized by anharmonic forces and eventually give rise to an instability of the lattice, resulting in a phase transition to another crystal structure.

3.3 Superconductivity in MgB_2

MgB_2 was found to be superconducting at 39 K in 2001 [18]. This is the highest T_c for a conventional superconductor. The material has a hexagonal

lattice with lattice parameters a=0.3086 nm and c=0.3524 nm (see fig. 3.8[1]).

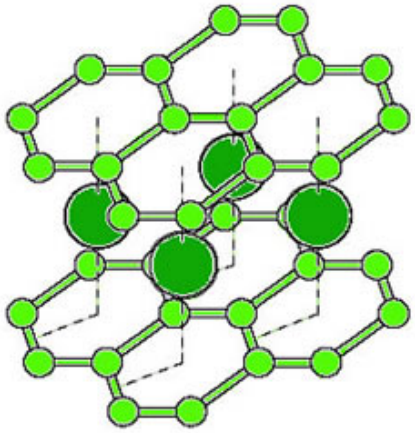

Figure 3.8: structure of MgB_2

The material is layered, it consists of alternating Mg- and B-planes, and therefore expected to be anisotropic. The T_c is unusually high for such a simple material. The previous record holder was crystalline Nb_3Ge with 23 K. MgB_2 is also extraordinary in the sense that it has two different energy gaps which open at the same temperature (39 K)[19].
MgB_2 has a graphite-like structure. The boron atoms in MgB_2 form honeycomb planes and magnesium atoms between the layers in the centers of the boron hexagons. The electrons of the B-atoms form σ-bonds in the B-planes and π-bonds between them. Not all the σ-bonds are occupied, because B has not enough electrons to fill 3 σ- and 1 π-bond. The σ and π electrons occupy different sites on the Fermi surface (see fig. 3.9).

Because the charge distribution of the σ-bonding states is not symmetrical with respect to the in-plane positions of B-atoms, the σ-bonding states couple very strongly to the in-plane vibration of the B-atoms (see fig. 3.10). These electrons form strong pairs with an average energy gap of 6.8 meV.

The π-bonding states form much weaker pairs with an average Δ of 1.8 meV (see fig. 3.11). Acting alone they would correspond to a T_c of 45 K and 15 K, respectively. But they cannot, and together they lead to a T_c of 39 K. This pairing is enhanced by the coupling to the σ-bonding states.
The Mg-atom is highly ionized. In fact the material can be written as

[1]The pictures in this section were taken from reference [19]

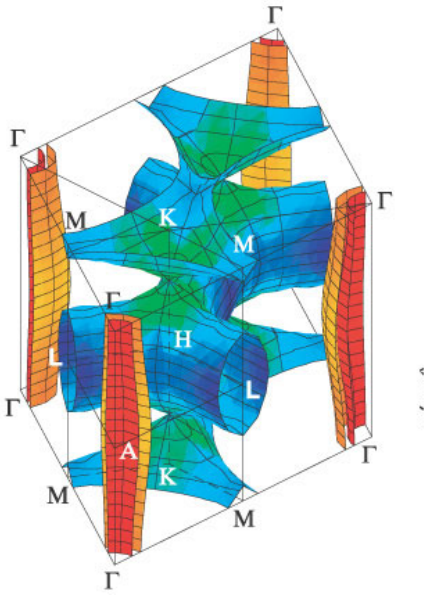

Figure 3.9: Fermi-surface of MgB_2. The cylinders on the edges correspond to the σ-states, the other parts to the π-states.

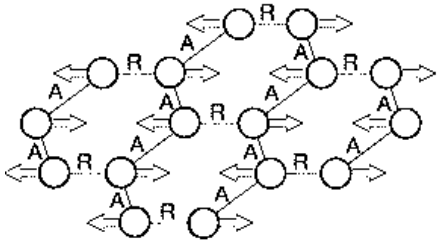

Figure 3.10: phonon mode of MgB_2

$Mg^{2+}B_2^-$. This charge is not used to form a covalent bond but spread diffusively over the crystal (as in a metal).

Isotope effect Boron naturally consists of ^{10}B and ^{11}B. So boron in MgB_2 consists of a mixture of both isotopes. But it is also possible to prepare MgB_2 with only ^{10}B or ^{11}B. $Mg^{10}B_2$ has a T_c of 40.2 K and $Mg^{11}B_2$ has a T_c of 39.2 K [20]. So the T_c depends on the mass of the atoms and therefore the material shows that the coupling mechanism involves phonons. It is also possible to use Mg-isotopes instead of B-isotopes. The effect is less than with

B-isotopes but it is present.

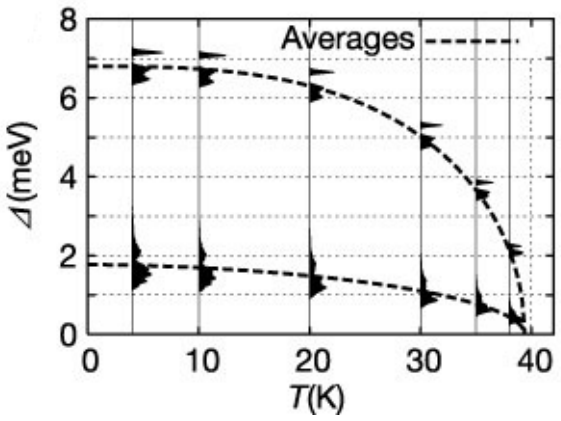

Figure 3.11: MgB_2 energy gap

Also MgB_2 seems to be close to a phase transition [21]. The B-B bond length in MgB_2 is significantly stretched with respect to the bond length in elemental boron (0.1764 nm in MgB_2 and 0.165 nm in B). This can be due to repulsive interactions between Mg and B ions. This explains the anharmonicity and high T_c.

3.4 Sample preparation

The NbN-samples were sputtered in the UHV, Z-400 and ATC on Si- and SiN-substrates. The base pressure in the Z-400 was approximately $2 \cdot 10^{-6}$mbar. No silver paint was used so that the substrate was not cooled by the underlying base plate. Used gas flows: 18% Ar and 10% N_2. $V_{DC} = 1.0$ kV. The sputter rate was approximately 2.5 nm/min.
The base pressure in the UHV was approximately $5{\cdot}10^{-9}$ mbar. The Ar- and N_2-pressures were parameters to be optimized. DC and RF power supplies were used. The Dc sputtering current was 220 mA. The RF power supply was used with 100 W or 200 W. The sputter rate was approximately 3 nm/min when using the DC power supply, 0.3 nm/min when using the RF power supply with 100 W and 1 nm/min when using the RF power supply with 200 W.
The base pressure in the ATC was typically $2 \cdot 10^{-7}$ Torr. The Ar and N_2 gas flows and the pressure can be varied individually and they are indicated in the chapter experimental results. Only a DC power supply was used. A

heater was used to heat the substrates to a certain temperature. The sputter rate was approximately 1 nm/min when using the NbN target without N_2 added and 0.75 nm/min when adding N_2. The sputter rate when using the Nb target was approximately 0.5 nm/min when using 100 mA and 1.8 nm/min when using 200 mA.
Some samples were structured with optical lithography. The length of the structure is 2.5 mm and the width 200 μm. The samples were etched using an ion beam etcher. During etching the samples were cooled with N_2.
The MgB_2-sample was made at Pennsylvania State University [2]. The dimensions were 5×5 mm. The thickness was 150 nm. It was structured with optical lithography. The length of the structure is 1 mm and the width 200 μm. The structuring caused problems because the structure had the same dimensions as the sample (or better, was slightly larger than the sample). So after development there was still remaining resist between the contact pads. It was necessary to separate the contact pads by scratching away the remaining resist with a knife before etching. The resulting contact were a bit damaged but they worked well.
The resistance of both the NbN and MgB_2 samples was measured in the PPMS in a conventional four point geometry. Electrical contacts were made with indium (on NbN) or with silver paint (on MgB_2 because In did not stick). For all samples R-T curves and R-H curves were measured. T_c was defined to be at 50 % of the value for R_0. R_0 is the resistance of the sample just above the transition. The transition width (ΔT_c) was measured between the data points at 20 % and 80 % of the value for R_0.

The choice of substrates The first samples (NbN-1 to NbN-8) were made on Si substrates, the other ones, except Nb samples, were made on SiN substrates. This is because it appeared that the N atoms were able to diffuse into the Si substrate. This caused strange boundary layers which are visible in the R-T curves. The R-T-curves showed a large jump around 200 K as can be seen for example in fig. 3.12. The two samples in the figure have a similar T_c and resistivity but the sample made on the Si substrate shows a jump where the sample made on the SiN substrate does not show anything in that region. So this problem can be avoided by the use of SiN substrates, where the N atoms are already present. T_c seems to be not affected by this problem.

[2]The sample was made by P. Orgiani.

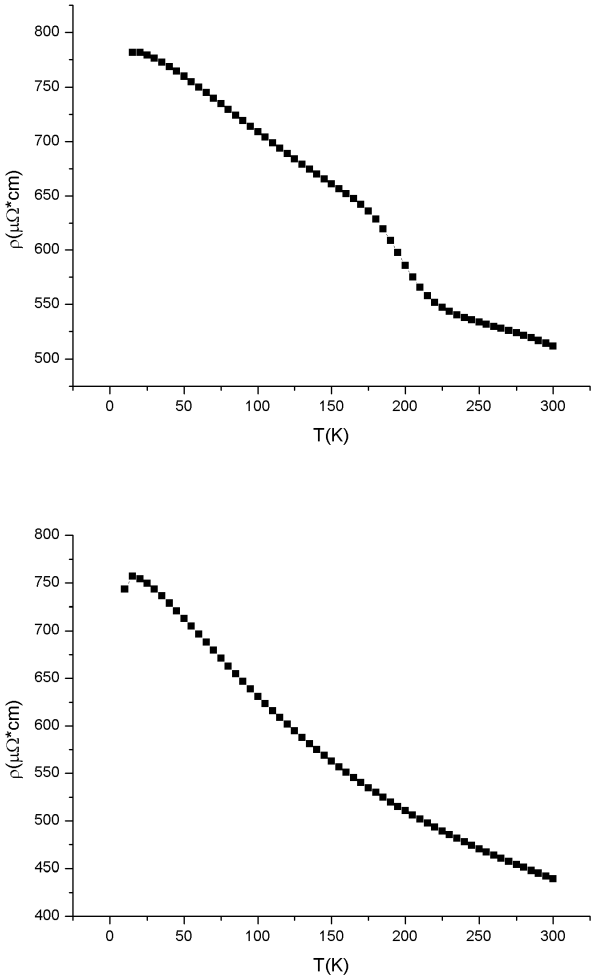

Figure 3.12: R vs. T curves (T=10-300K) for 2 samples with comparable resistivity and T_c. **Top:** sample made on Si substrate. **Bottom:** sample made on SiN substrate. The sample made on the Si substrate shows a jump around 200 K where the sample made on the SiN substrate doesn't show anything.

3.5 Sample characterization

The composition, crystal structure and thickness of the sputtered NbN films was measured by X-ray diffraction, RBS (Rutherford back scattering) and Auger electron spectroscopy (AES). X-ray diffraction was used to examine

the thickness and crystal structure of the samples. All examined samples showed a cubic structure, but the exact crystal structure could not be determined because of the thin samples (all samples were thinner than 50 nm). Some samples appeared to be very inhomogeneous. These were the samples made with the NbN target in the ATC which also showed very broad transitions (sample ID's NbN-22, NbN-23, NbN-25 and NbN-27).
The composition of one of the samples was investigated by RBS (Rutherford back scattering). The composition of the sample was difficult to determine because the mass of the Nb atoms and the N atoms is very different. It is clear that Nb and N atoms are present in the sample, and some Ar, but the exact composition remains a bit uncertain. However, it should be close to Nb_1N_1.
The composition of a material can be also studied using electron spectroscopy.[3]. The electrons used in this method can penetrate the material only a short distance (few nm). A number of methods can be used. The one used for this project is called Auger electron spectroscopy (AES). It was useful to determine the amount of N atoms in the samples, which was not possible to do with RBS. It is used to identify the elements at the surface. For this technique the incident electrons have an energy of a few keV. They can excite an atom by knocking one of its electrons out of its shell. The hole in the shell is filled by one of the electrons from a higher level. The energy lost by this electron can be released as a photon or an electron. The electrons are used in the Auger process. These electrons have well known energies which are different for each element. Therefore it is possible to determine the elements at the surface. To obtain a depth profile of the sample it is possible to etch a layer away after measuring the surface and create a new surface to measure. The AES results are given in section 4.5.

[3]The material in this paragraph was taken from reference [22]

Chapter 4

Experimental results

4.1 Literature guided optimalization of T_c

The NbN films were deposited by reactive sputtering. We are looking for methods to make samples with the desired properties, i.e. mainly the highest T_c. The properties of NbN are found to depend on the sputter conditions. The curve of target voltage against partial nitrogen pressure at constant argon pressure has an S-shape and shows a hysteresis effect [23]. It was found that the films deposited at the points on the elbows of the hysteresis curve have the highest T_c. So for NbN samples with high T_c's the hysteresis curve for the UHV should be determined. Measurements of target voltage as function of partial nitrogen pressure however showed no hysteresis and no S-shape. The results can be seen in fig. 4.1 at two different Ar pressures.

Also shown (fig. 4.2) is the effect of keeping the total pressure constant and varying the partial N_2 pressure. This means that the Ar pressure and the N_2 had to be adjusted at the same time. It was only possible to register the total pressure, which causes large difficulties in regulating the pressure with reasonable accuracy. This is the reason for the error bars in the graph. The graph shows again no hysteresis.

It is also possible to leave the N_2 pressure constant and vary the Ar pressure. The result is shown in fig. 4.3. The upward curvature at low Ar pressures is an expected feature. There is no sign of hysteresis.

4.2 Z400 results

The first two samples were made in the Z400. The films were made on Si substrates. The thicknesses were 50 nm and 5 nm respectively. After deposition they were patterned using the standard procedure. Thicknesses

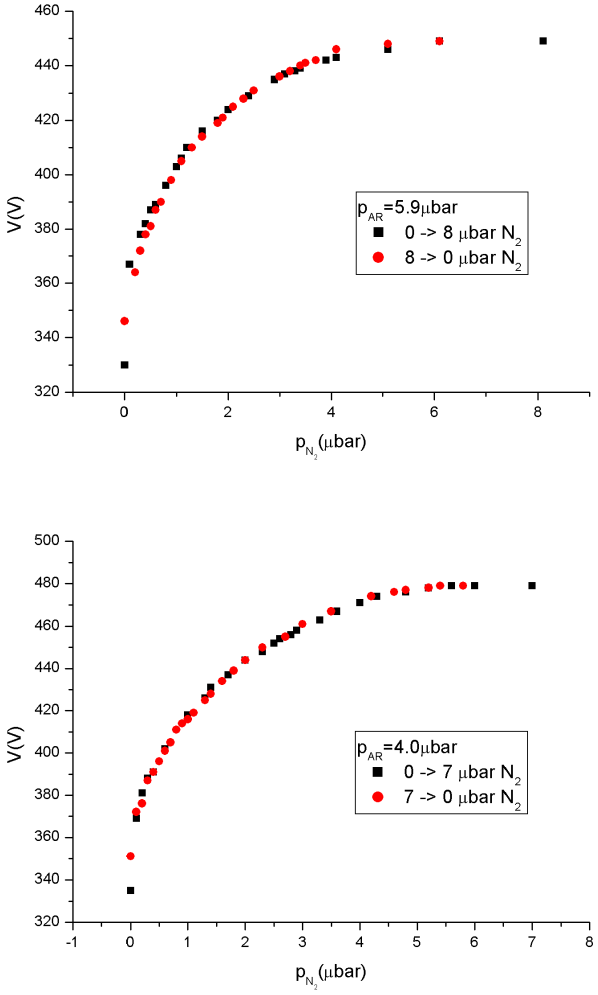

Figure 4.1: Voltage over Nb target as function of N_2 partial pressure for two different constant Ar partial pressures. **Top:** Ar pressure of 5.9 μbar. **Bottom:** Ar pressure of 4.0 μbar. Current was 220 mA in both cases. The curves show no hysteresis.

were confirmed by X-ray diffraction. For both samples the R vs. T and R vs. H curves were measured. The results for the 50 nm sample are shown in fig. 4.4 and those for the 5 nm sample in fig. 4.5. Sample characteristics are given in table 4.1. $\xi(0)$ is calculated from dH_{c2}/dT using equation 2.29. During this project the Z400 samples became suspected of containing large amounts of carbon, causing T_c to be higher than expected. One of the next

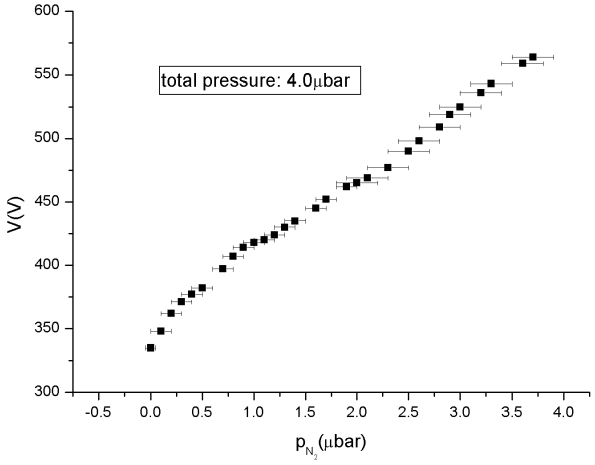

Figure 4.2: Voltage over Nb target as function of N_2 partial pressure while keeping the total pressure constant (4.0 μbar). This means that also the Ar partial pressure had to be adjusted. Current was kept constant at 220 mA. The curve shows no hysteresis.

sample ID	thickness (nm)	T_c (K)	R_0 ($\mu\Omega$*cm)	$R_\square$ (Ω)	dH_{c2}/dT (T/K)	$\xi(0)$ (nm)
NbN-1	50	10.5	239	47.8	-2.15	3.8
NbN-2	5	4.6	738	1416	-2.54	5.3

Table 4.1: sample characteristics for the Z400 samples

sections will be devoted to this problem.

As can be seen in the table, the T_c decreases with increasing sheet resistance ($R_\square$). The sheet resistance is defined as

$$R_\square = \frac{\rho}{d} \tag{4.1}$$

where d is the thickness of the sample. This can be understood within the framework of the theory of weak localization. The T_c is reduced by localization. This is because the Coulomb repulsion between electrons is enhanced and the electron density of states is depressed. Both tend to lower T_c. The effects of localization on 2D superconductors was studied theoretically by Maekawa and Fukuyama (MF) [24][25]. The result MF obtained by perturbation theory was

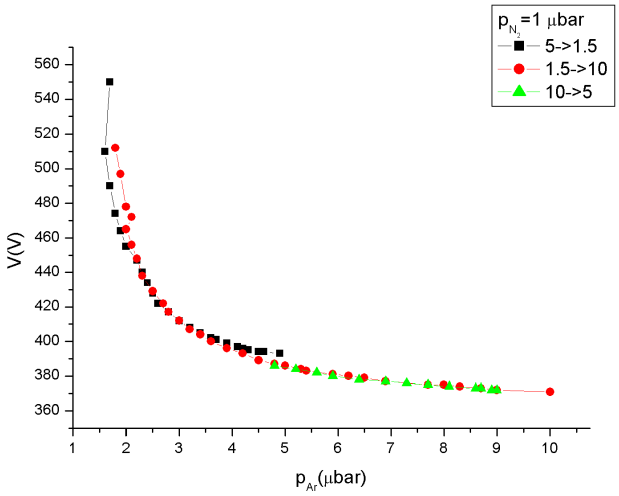

Figure 4.3: Voltage over Nb target as function of Ar partial pressure. N_2 pressure was kept constant at 1 μbar. Current was 220 mA. The curve shows no hysteresis. The upward curvature at low Ar pressures is a normal feature at low pressures.

$$\ln\left(\frac{T_c}{T_{c0}}\right) = -\frac{1}{2}\frac{g_1 N(0) e^2 R_\square}{2\pi^2\hbar}\left[\ln\left(5.5\frac{\xi_0}{l}\frac{T_{c0}}{T_c}\right)\right]^2 - \frac{1}{3}\frac{g_1 N(0) e^2 R_\square}{2\pi^2\hbar}\left[\ln\left(5.5\frac{\xi_0}{l}\frac{T_{c0}}{T_c}\right)\right]^3 \tag{4.2}$$

The first term describes the reduction of the density of states and the second term a correction to the electron-electron interaction. T_{c0} denotes the bulk T_c value, l the mean free path and $g_1 N(0)$ is the effective coupling constant. This can be used to determine if the T_c reduction is due to weak localization. ξ_0 is the BCS coherence length, which was not measured but can be roughly calculated by the equation

$$\xi(0) = 0.855\sqrt{\xi_0 l} \tag{4.3}$$

The mean free path is supposed to be of the order of the interatomic distance (4 Å) and $\xi(0)$ is taken to be the mean of the $\xi(0)$'s of the 2 samples (roughly 4 nm). So ξ_0 is approximately 55 nm and $\xi_0/l \approx 135$. T_{c0} is expected to be slightly higher than T_c for a 50 nm sample, between 10.5 K and 11 K. $g_1 N(0)$ should be of order unity for the theory to be applicable. Fig. 4.6 shows the

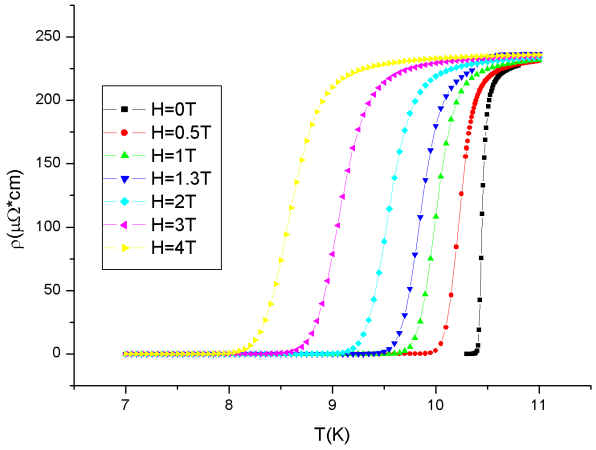

Figure 4.4: R vs. T at different magnetic fields H for a 50 nm thick NbN sample made in the Z400

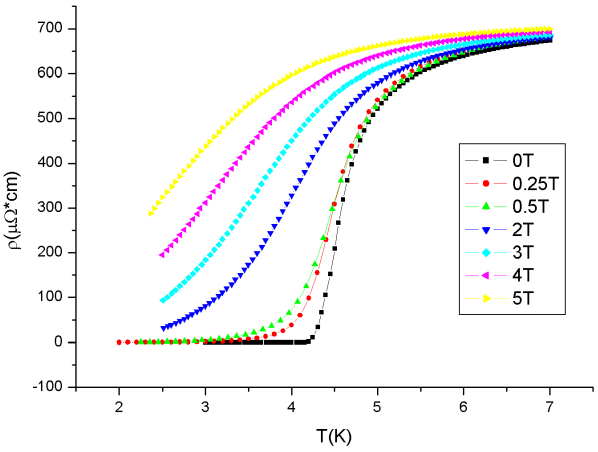

Figure 4.5: R vs. T at different magnetic fields for a 5 nm thick sample made in the Z400

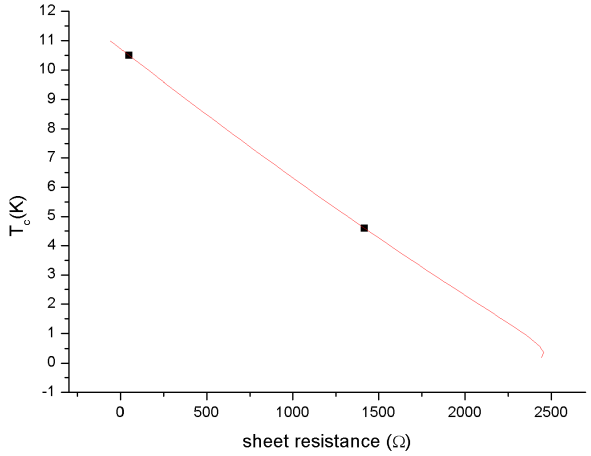

Figure 4.6: T_c/T_{c0} vs. $R_\square$ for the Z400 data points, with fit to theory. T_{c0} is 10.7K

results of the fitting procedure. It gives 10.7 K as T_{c0} and 0.30 as value for $g_1N(0)$. This seems to be reasonable. This means that the weak localization theory can be a good model to explain the T_c reduction. It is not possible to base definitive conclusions on only two data points but it is an indication that lower T_c's can be expected in thin films.

4.3 UHV results

The following samples were made in the UHV. The sputter conditions are given in table 4.2. All samples were DC sputtered except samples NbN-14, NbN-15, NbN-16 and NbN-17 which were RF sputtered. After sputtering most samples were structured. R vs T and R vs H curves were measured. A typical measurement is shown in figure 4.7. Data are given in table 4.3. Data for a 50 nm thick Nb sample are added for comparison. The samples NbN-4, NbN-5 and NbN-6 were suspected of being contaminated with O_2 because the T_c was very low and there was a leak in the sputtering system.

As can be seen, T_c for all samples is lower than that in the Z400 for comparable thickness. The maximum T_c measured is 8.3 K, which is even lower than that of pure Nb made in the same system. The question arises if this is also caused by weak localization. This would mean that a higher T_c could be reached with a thicker sample. In order to check this the data

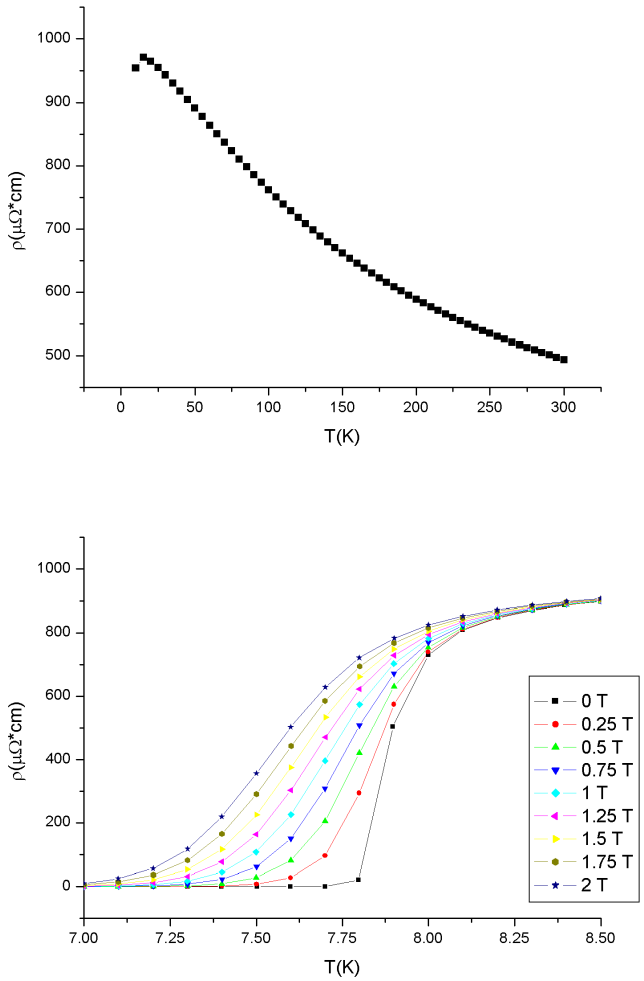

Figure 4.7: typical R vs. T curves for a UHV sample. **Top:** T=10-300 K. **Bottom:** T=7.0-8.5 K at different magnetic fields.

sample ID	p_{Ar} (μbar)	p_{N_2} (μbar)	sputter time	thickness (nm)	I (mA)	V (V)
NbN-3	5	1	7 min.	25	200	490
NbN-4	4	2	6 min. 40 s.	25	220	494
NbN-5	4	2	6 min. 40 s.	25	220	442
NbN-6	5	1	6 min. 40 s.	25	220	-
NbN-7	4	0.5	13 min. 20 s.	40	220	397
NbN-8	4	1	13 min. 20 s.	40	220	-
NbN-9	5	1	20 min.	64	220	401
NbN-10	4.5	1	16 min. 40 s.	50	220	391
NbN-11	5.5	1	16 min. 40 s.	50	220	387
NbN-12	6	1	16 min. 40 s.	50	220	383
NbN-13	7	1	16 min. 40 s.	50	220	382
NbN-14	4	1	15 min.	4.5	100 W	RF
NbN-15	5	1	15 min.	5.5	100 W	RF
NbN-16	6	1	15 min.	6.5	100 W	RF
NbN-17	6	1	46 min.	51.5	200 W	RF

Table 4.2: sputter conditions for the UHV samples

points of the UHV samples are plotted in the same graph as the Z400 points (fig. 4.8). Assumed is that the weak localization theory is valid in this case and that $g_1N(0)$ has the same value as in the case of the Z400 samples (0.30). Curves are drawn which represent fitting curves for certain data points. In this way, a value for T_{c0} is determined for all samples. In fig. 4.9 T_{c0} is given as function of the partial N_2-pressure used to fabricate them. Three samples have a lower T_c than expected. They are suspected to be contaminated with O_2. These samples have a different symbol. Another sample was sputtered under RF conditions instead of DC. This sample has a different symbol too.

The conclusion from fig. 4.9 must be that it is not possible to have a T_c higher than 9 K with these samples, since even the values for T_{c0} do not exceed 8.9 K. The low T_c is not explained by weak localization and thicker samples are not expected to have much higher T_c. Also T_{c0} seems to vary not very much when the sputtering conditions differ.

4.4 ATC results

In the ATC 2 different targets can be used. The first one is a NbN target. This target was used initially without any N_2 added in the sputter gas, as

sample ID	thickness (nm)	T_c (K)	dH_{c2}/dT (T/K)	$\xi(0)$ (nm)	R_0 ($\mu\Omega$*cm)	$R_\square$ (Ω)
NbN-3	25	8.3	-3.5	3.4	390	156
NbN-4	25	4.5	-	-	1250	500
NbN-5	25	5.1	-5.8	3.3	1050	420
NbN-6	25	5.4	-4.1	3.8	400	160
NbN-7	40	4	-	-	-	-
NbN-8	40	4.8	-	-	-	-
NbN-9	64	8.2	-5.0	2.8	760	119
NbN-10	50	7.3	-3.8	3.5	624	125
NbN-11	50	8.1	-	-	650	130
NbN-12	50	7.9	-6.3	2.6	970	194
NbN-13	50	6.9	-9.6	2.2	2097	420
NbN-14	4.5	<2	-	-	-	-
NbN-15	5.5	<2	-	-	-	-
NbN-16	6.5	<2	-	-	-	-
NbN-17	51.5	6.7	-4.4	3.4	1100	213
Nb	50	8.6	-0.40	9.8	10.7	2.14

Table 4.3: sample characteristics of the UHV samples

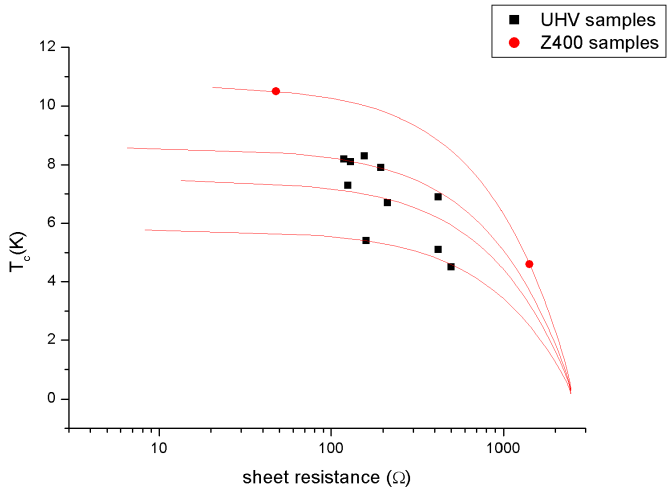

Figure 4.8: T_c vs. $R_\square$ for the UHV data points, with fit to theory. The fit shows that the values for T_{c0} are between 5.7 K and 8.9 K. T_{c0} does not depend very strongly on sputtering conditions and the low T_c's are not explained by weak localization.

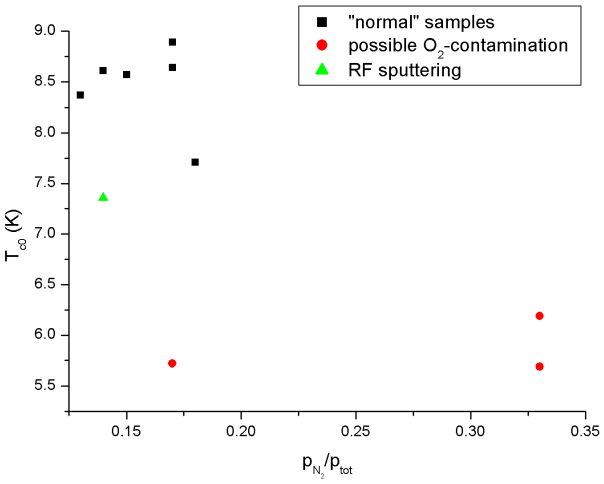

Figure 4.9: T_{c0} vs. p. The highest T_c can be achieved when p_{N_2}/p_{tot} is about 0.17

sample ID	pressure (mTorr)	Ar gas flow (sccm)	N_2 gas flow (sccm)	T (°C)	I (mA)	thickness (nm)
NbN-18	4	25	0	RT	100	19
NbN-20	4	25	0	500	100	16
NbN-22	4	25.1	0	700	100	13
NbN-23	4	24.9	0	700	100	41
NbN-25	4	25.2	0	790	100	41
NbN-27	5	24.8	0	790	100	43
NbN-31	4	50	0.5	700	100	35
NbN-32	4	50	2.5	700	100	27
NbN-33	4	50	1	700	100	32

Table 4.4: sputter conditions for ATC samples made using the NbN target

all the necessary N atoms should be already present. The other one is a Nb target which can be used with N_2 added to the sputtering gas.

NbN target

The following samples were made in the ATC using a NbN target. The sputter conditions are given in table 4.4 and the measured data in table 4.5. The first sample was made without heating the substrate or addition of N_2. It had no T_c above 2 K. To get a higher T_c it was necessary to heat the substrate. Samples were made with the substrates at 500 °C, 700 °C and 790 °C. The samples sputtered at 700 °C had the highest T_c. But these transitions were very broad, more than 5 K, see for example the graph of sample NbN-23 in fig. 4.10.

Sputtering at a higher pressure made it only worse. This problem was solved by the addition of N_2 in the sputter gas. Apparently there is some loss of N atoms. These had to be added again. Addition of 1%, 2% and 5% N_2 was tried. The samples were not structured, except the first one. The maximum T_c for this target was 11.7 K.

Nb target

The following samples were made in the ATC using a Nb target. The sputter conditions are given in table 4.6 and the measured data in table 4.7. Because it was profitable to heat the substrates when using the NbN target also for the Nb target the substrates were heated. Trying to make a sample at room temperature showed that the T_c tends to become lower if the sample was

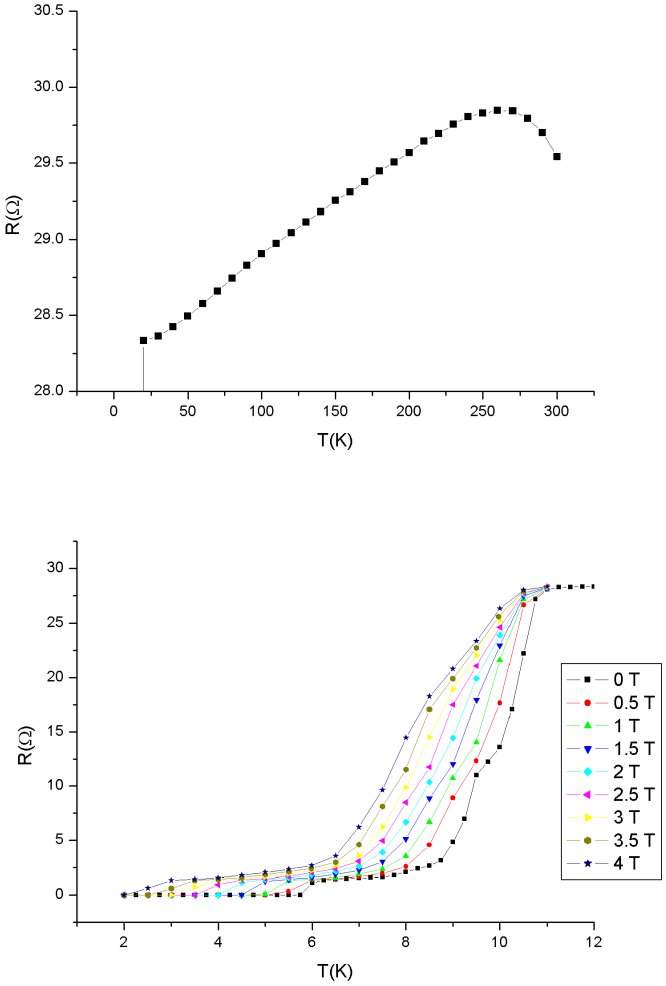

Figure 4.10: R. vs. T for sample NbN-23. The high temperature graph shows non-monotonic behavior and the transition is very broad. Apparently this sample is not homogeneous. **Top:** T=10-300 K. **Bottom:** T=2-10 K at different magnetic fields.

sputtered at lower temperatures but not as much as with the NbN target. The maximum T_c for this target was 12.9 K. The samples are not structured, except the last one.

sample ID	thickness (nm)	T_c (K)	ΔT_c (K)	dH_{c2}/dT (T/K)	$\xi(0)$ (nm)
NbN-18	19	-	-	-	-
NbN-20	16	7.3	0.5	-1.62	5.3
NbN-22	13	8.4	1.7	-1.60	5.0
NbN-23	41	10.0	1.5	-1.94	4.1
NbN-25	41	7.5	5.1	-1.65	5.2
NbN-27	43	7.1	5.9	-1.57	5.4
NbN-31	35	11.7	0.4	-1.97	3.8
NbN-32	27	11.7	0.3	-1.92	3.8
NbN-33	32	10.4	0.3	-2.23	3.8

Table 4.5: sample characteristics of ATC samples made using the NbN target.

sample ID	pressure (mTorr)	Ar gas flow (sccm)	N_2 gas flow (sccm)	T (°C)	I (mA)	thickness (nm)
NbN-21	4	25	12.1	RT	100	12
NbN-26	4	25	6.0	790	100	19
NbN-28	4	24.8	7.0	790	100	20
NbN-29	4	25	3.2	790	100	22
NbN-30	4	25	2.5	700	100	23
NbN-34	4	25	2.5	RT	200	86
NbN-35	4	25	2.5	500	200	75
NbN-36	4	25	2.5	250	200	75
NbN-37	4	25	2.5	500	200	83

Table 4.6: sputter conditions for ATC samples made using the Nb target

sample ID	thickness (nm)	T_c (K)	ΔT_c (K)	dH_{c2}/dT (T/K)	$\xi(0)$ (nm)
NbN-21	12	-	-	-	-
NbN-26	19	9.2	0.3	-3.07	3.4
NbN-28	20	8.9	0.4	-3.38	3.3
NbN-29	22	11.1	0.6	-3.43	2.9
NbN-30	23	11.5	0.5	-3.18	3.0
NbN-34	86	9.5	0.5	-11.8	1.7
NbN-35	75	12.9	0.3	-5.69	2.1
NbN-36	75	12.3	0.3	-7.0	2.0
NbN-37	83	11.7	0.3	-7.66	1.9

Table 4.7: sample characteristics of ATC samples made using the Nb target.

4.4.1 Nb sample

There was one Nb sample made in the ATC. The conditions were: pressure 4 mTorr, Ar gas flow 24.9, no N_2, sputtered at room temperature, current 100 mA. The sample was sputtered for 45 min. and the thickness was 40 nm. A Si substrate was used, it is not possible to use a SiN substrate. The T_c was 3.8 K which is not very high. The sample was not structured.

4.5 Auger electron spectroscopy (AES)

As can be seen in the previous sections, the maximum T_c in the Z400 is much higher than in the UHV. This is counterintuitive. Naive thinking would shown that it is the other way around. The vacuum in the Z400 is much worse than in the UHV (roughly 3 orders of magnitude) and therefore the Z400 samples are expected to be more oxidized. Oxidation makes the T_c lower. And as in the UHV the samples cannot be heated, which would make the T_c higher. The question is: why is the T_c of the Z400 samples as high as it is. It could be that the amount of carbon is much higher in the Z400 samples than in the UHV samples, as carbon tends to enhance the T_c of NbN. So this needs to be checked.
The amount of carbon was checked by AES. Two samples are made, one in the UHV and the other in the Z400. Both are approximately 50 nm thick. AES was performed within the Department of Materials Science at Delft University of Technology.[1] In Fig. 4.11 the results for the UHV sample are

[1]The measurements were performed by C. Kwakernaak and W.G. Sloof.

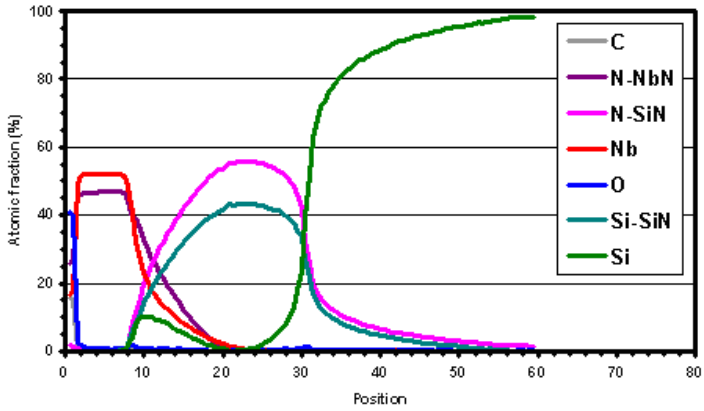

Figure 4.11: AES for the UHV sample. On the left side are the surface layers and on the right side the composition of the substrate is given. The interesting part is the part in between, the NbN layer between 0 and 10 on the x axis scale. The only elements that are detected are Nb, N and a small amount of O and C. This shows that the material that was made by sputtering in the UHV is NbN without important amounts of NbC.

shown. It shows the composition as function of depth. The left side is the surface side and the right side is the substrate side. On the surface there is mainly O and C, as expected. Then comes the NbN layer.In this layer there is mainly Nb and N and only small amounts of C and O (O approximately 1%, C less). The next layer is SiN with Si and N and small amounts of C and O and finally a Si layer.

In Fig. 4.12 the results for the Z400 sample are shown. The graph is mostly the same as for the UHV sample except one interesting thing. In the NbN part of the graph is one extra line visible which shows that there a considerable amount of C in the sample. The amount is approximately 9% at the surface and increases with increasing depth. At the NbN-SiN interface it is 18%. Also the amount of N in the NbN is less. Actually the NbN can better be described as $NbC_{1-x}N_x$ with x=0.7-0.8. This is the composition which gives the highest T_c in the $NbC_{1-x}N_x$ system [9] [16]. This is thought to be the explanation of the unexpectedly high T_c of the Z400 samples.

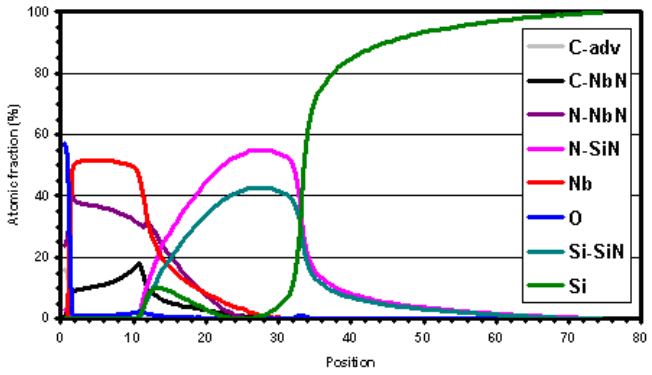

Figure 4.12: AES for the Z400 sample. The graph looks similar to fig. 4.11 but in this sample a large amount of carbon is detectable in the NbN layers. This shows that the material is not really NbN but can better be described as $NbC_{1-x}N_x$ with x=0.7-0.8.

Chapter 5

Conclusions

The following conclusions can be drawn:

- The first 2 samples from the Z400 showed that T_c becomes lower as the samples become thinner. This is probably caused by weak localization effects. The bulk T_c should then be 10.7 K.
- The attempts to increase T_c of the UHV samples result in a T_c not higher than 8.3 K. Both DC and RF sputtering were tried and various N_2 pressures were applied. The fact that the T_c of the UHV samples is lower than that of the Z400 samples is not caused by weak localization effects. Provided that the theory is valid the bulk T_c does not exceed 9 K.
- The high T_c of the Z400 samples is caused by addition of carbon. The AES measurement showed that the Z400 samples contained roughly 15 % C. The UHV samples contained less than 1 % C. The high amount of C in the Z400 samples caused the relatively high T_c. The carbon originates from oil streaming back from the pumps.
- It is possible to make samples with high T_c's in the ATC. It is necessary to use a heater. Both a Nb target and a NbN target were used. The highest T_c using the NbN target was 11.7 K (sputtered at 700 °C and 1% N_2 added). The highest T_c using the Nb target was 12.9 K (sputtered at 500 °C and using 10% N_2). Both targets have to be optimized further.

Appendix A

MgB_2

The MgB_2 sample was first patterned and then measured. First the R-T curve at 10K-300K was determined (see fig. A.1).

In fig. A.1 is visible that T_c of this sample is approximately 40 K. The sample showed metallic behavior above the transition temperature. To determine T_c R-T was measured in the vicinity of 40 K (see fig A.2).

As can be seen the T_c is 40.0 K. The transition width is less than 0.1 K. Also the R-H curves were measured for different configurations. The sample was measured in perpendicular field (fig. A.3), in parallel field with strip perpendicular to the field (fig. A.4) and in parallel field with the strip parallel to the field too (fig. A.5).

As can be seen the resistivity in the normal state in the measurement with the strip and the field parallel is higher than that with the perpendicular field. This is probably some sample degradation as the measurements were not performed directly after each other. In each case it is no contact problem. It also caused a T_c lowering of 0.1 K. Particularly in the measurement with perpendicular field there is a large magnetoresistance in the normal state visible. This is believed to be caused by unreacted Mg in the MgB_2 sample [26]. In fig. A.6 a H vs. T plot is shown for all three configurations. From this plot can be concluded that the sample is anisotropic as could be expected from the crystal structure. At higher temperatures (35-40 K) the curve has an upward curvature which was not expected. This is in agreement with literature but the meaning is not yet clear [27].

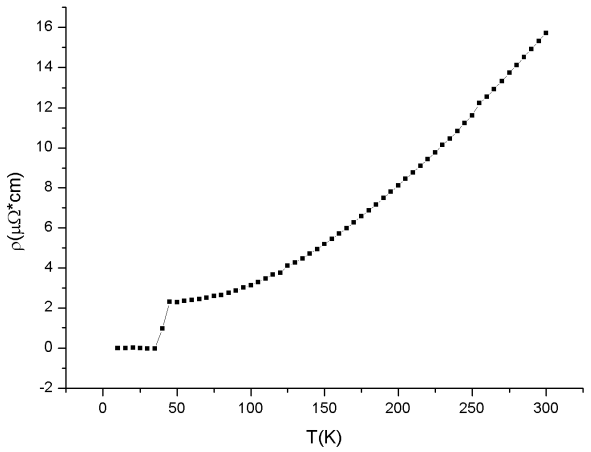

Figure A.1: MgB_2: resistivity vs. temperature, 10 K-300 K

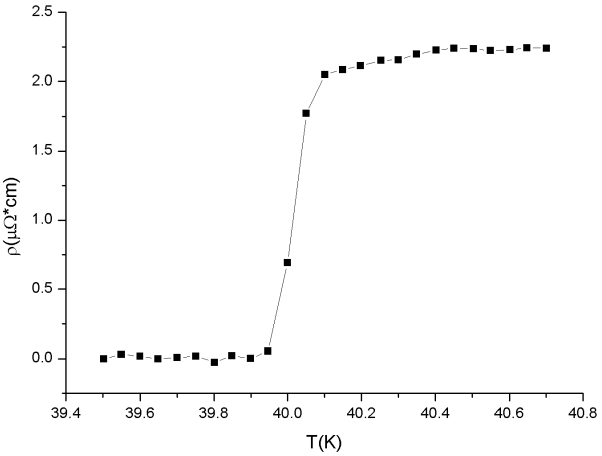

Figure A.2: MgB_2: closer look at T_c

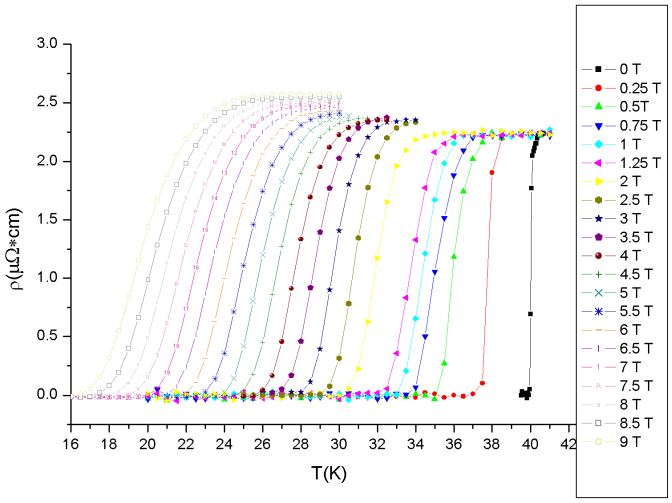

Figure A.3: MgB_2: resistivity vs. temperature in perpendicular field at different magnetic fields.

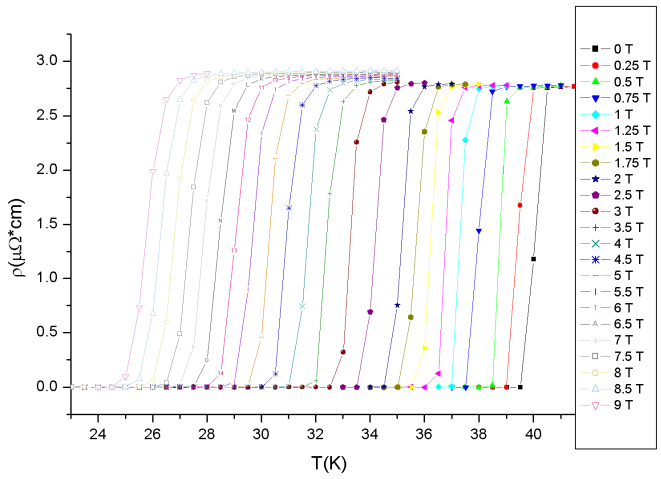

Figure A.4: MgB_2: resistivity vs. temperature in parallel field at different magnetic fields. Strip was mounted perpendicular to the field.

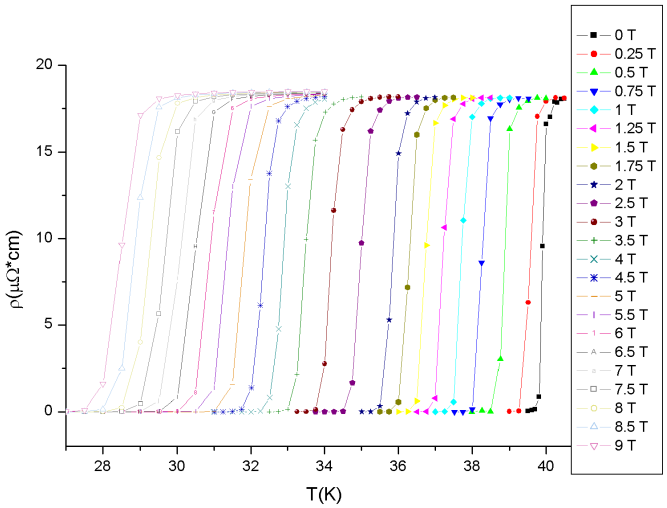

Figure A.5: MgB_2: resistivity vs. temperature in parallel field at different magnetic fields. Strip was mounted parallel to the field.

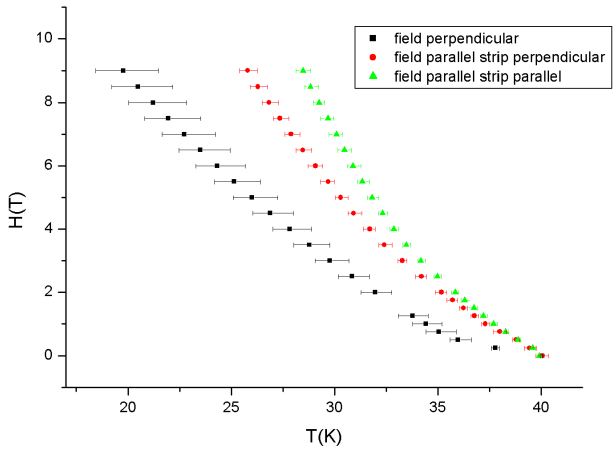

Figure A.6: MgB_2:H vs. T. Error bars mean transition widths.

Bibliography

[1] H. Kamerlingh Onnes, Leiden Comm. **120b**, **122b**, **124c** (1911)

[2] M. Tinkham, Introduction to Superconductivity, Krieger Publishing Company, Malabar, Florida (1980)

[3] W. Meissner, R. Ochsenfield, Naturwiss. **21**, 787 (1933)

[4] F. and H. London, Proc. Roy. Soc. (London) **A149**, 71 (1935)

[5] L. N. Cooper, Phys. Rev. **104**, 1189 (1956)

[6] J. Bardeen, L. N. Cooper and J. R. Schrieffer, Phys. Rev. **106**, 162 (1957)

[7] J. Bardeen, L. N. Cooper and J. R. Schrieffer, Phys. Rev. **108**, 1175 (1957)

[8] V.L. Ginzburg and L.D. Landau, Zh. Eksperim. Theor. Fiz. **20**, 1064 (1950)

[9] L.E.Toth,'Transition metal carbides and nitrides'. Academic Press, New York. (1971)

[10] G.Oya and Y.Onodera, J.Appl.Phys. **45**, 1389-1397 (1974)

[11] G.Brauer and E.Esselborn, Z.Anorg.Allg.Chem. **309**, 151 (1951)

[12] R.W.Guard, J.W.Savage and D.G.Swarthout, Trans. AIME **239**, 643 (1967)

[13] E.C Ethridge, S.C.Erwin and W.E.Pickett, Phys. Rev. B **53**, 12563 (1996)

[14] R.Marchand, F.Tessier and F.J. DiSalvo, J.Mater.Chem. **9**, p.297-304 (1999)

[15] G.Oya and Y.Onodera, J.Appl.Phys. **47**, 2833-2840 (1976)

[16] B.T.Matthias, Phys.Rev. **92**, p.874 (1953)

[17] J.C.Phillips, Phys. Rev. Lett. **26**(10), p.543-546 (1971)

[18] J.Nagamatsu, N.Nakagawa, T.Muranaka, Y.Zenitani and J.Akimitsu, Nature **410**, 63-64(2001)

[19] H.Choi, D.Roundy, H.Sun, M.Cohen and S.Louie, Nature **418**, 758-760(2002)

[20] D.G.Hinks, H.Claus and J.D.Jorgensen, Nature **411**, 457-460(2001)

[21] T.Yildirim *et al.* Phys. Rev. Lett. **87**, 037001 (2001)

[22] J.R.Hook and H.E.Hall, Solid state physics, second edition, 1991 by Wiley

[23] K.L.Westra, M.J.Brett andJ.F.Vaneldik, J.Vac.Sci.Technol.A 8 1288-1293 (1990)

[24] S.Maekawa and H.Fukuyama, J.Phys.Soc.Jpn. **51**, 1380 (1981)

[25] M.R.Beasley and J.M.Graybeal, Phys. Rev. B **29**(7), p.4167-4169 (1984)

[26] K.H.Kim *et al.* Phys. Rev. B **66**, 020506(R) (2002)

[27] S.L.Bud'ko *et al.* Phys. Rev. B **63**, 220503(R) (2001)